arXiv:1510.08655v2 [cond-mat.str-el] 8 Mar 2016

Heisenberg antiferromagnet on the Husimi lattice

H. J. Liao,[1] Z. Y. Xie,[1,2] J. Chen,[1] X. J. Han,[1] H. D. Xie,[1] B. Normand,[2] and T. Xiang[1,3,*]

[1] *Institute of Physics, Chinese Academy of Sciences, P.O. Box 603, Beijing 100190, China*
[2] *Department of Physics, Renmin University of China, Beijing 100872, China*
[3] *Collaborative Innovation Center of Quantum Matter, Beijing 100190, China*

(Dated: March 9, 2016)

We perform a systematic study of the antiferromagnetic Heisenberg model on the Husimi lattice using numerical tensor-network methods based on Projected Entangled Simplex States (PESS). The nature of the ground state varies strongly with the spin quantum number, S. For $S = 1/2$, it is an algebraic (gapless) quantum spin liquid. For $S = 1$, it is a gapped, non-magnetic state with spontaneous breaking of triangle symmetry (a trimerized simplex-solid state). For $S = 2$, it is a simplex-solid state with a spin gap and no symmetry-breaking; both integer-spin simplex-solid states are characterized by specific degeneracies in the entanglement spectrum. For $S = 3/2$, and indeed for all spin values $S \geq 5/2$, the ground states have 120-degree antiferromagnetic order. In a finite magnetic field, we find that, irrespective of the value of S, there is always a plateau in the magnetization at $m = 1/3$.

PACS numbers: 75.10.Jm, 75.10.Kt, 75.50.Ee

I. INTRODUCTION

The investigation of low-dimensional quantum antiferromagnets has long been one of the most active frontiers in condensed matter physics. One of the most remarkable advances in the understanding of one-dimensional quantum spin systems is Haldane's conjecture [1, 2], that quantum Berry-phase effects cause the low-energy behavior of Heisenberg chains to depend strongly on the parity of $2S$. Half-odd-integer spin chains have gapless excitations and power-law decay of their spin correlation functions, whereas integer-spin chains have a finite excitation gap (the "Haldane gap") and exponentially decaying spin correlations. In fact Lieb, Schultz, and Mattis were first to prove that the excitation gap for half-odd-integer spin chains is bounded only by the system size ($\Delta \propto 1/L$) [3, 4].

The Haldane conjecture has inspired extensive theoretical studies, especially on integer-spin systems. Affleck, Kennedy, Lieb, and Tasaki (AKLT) provided the first rigorous example of a model with a unique ground state, a gap, and exponentially decaying spin correlation functions [5, 6]. It was later found that AKLT states exhibit several exotic features, such as a nonlocal "string order" and edge states, which are properties of all states within the same Haldane phase [7]. A theoretical framework for understanding these topological properties has been developed recently [8, 9] and used to classify all one-dimensional gapped systems [10–13].

Extensions of the understanding brought by the Haldane conjecture have long been sought for quantum spin systems in all dimensions higher than 1. The Lieb-Schultz-Mattis theorem was extended to higher dimensions by Hastings [14]. The AKLT construction can be extended to all higher dimensions in the form of simplex-solid states [15], where the two-site $S = 1/2$ bond singlet of the AKLT state is generalized to an N-site simplex singlet. As for the AKLT states, the simplex-solid state is an exact ground state of a many-body Hamiltonian, usually with a gap to all low-energy excitations. The wave function of a simplex-solid state can be represented by the Projected Entangled Simplex States (PESS) [16], providing the foundation for the numerical tensor-network technique we employ here. However, while the integer-spin case appears to have a number of higher-dimensional analogs, it has remained unclear whether any quantum spin system in dimension $d > 1$ can be simultaneously gapless, non-magnetic, and not break any other symmetries (particularly translational).

In this context, innumerable studies have been performed of highly frustrated models in two dimensions, including the triangular, Shastry-Sutherland, J_1-J_2 square, checkerboard, J_1-J_2-J_3 honeycomb, and other geometries, as well as of the pyrochlore lattice in three dimensions. However, the most challenging and enigmatic frustrated system of all has turned out to be the nearest-neighbor $S = 1/2$ Heisenberg model on the (two-dimensional) kagome lattice, due to the strong intrinsic frustration of this geometry. Despite extensive analytical and numerical efforts for almost three decades, the nature of the ground state and the existence of a spin gap remain as open questions, with primary candidates including several types of valence-bond crystal [17], different gapped Z_2 spin liquids [18], and a gapless, algebraic quantum spin liquid [19]. Recently, and in part with a view to solving this conundrum, more attention has also been paid to kagome Heisenberg antiferromagnets with higher spins [20, 21]. Various proposals have been put forward for the spin-1 case, including the hexagonal singlet solid state [22], the resonating AKLT loop state [23, 24], and the trimerized simplex-solid state [25–27], among which the last has the best variational energy [26, 27]. For the

* txiang@iphy.ac.cn

$S = 2$ case, a coupled-cluster calculation suggested that the ground state has $\sqrt{3} \times \sqrt{3}$ antiferromagnetic order [28], whereas the infinite Projected Entangled Pair States (iPEPS) algorithm indicates a (topologically trivial) spin liquid with a spin gap and no symmetry breaking [21].

The Husimi lattice [29], shown in Fig. 1(a), is an infinitely nested set of corner-sharing triangles. Although the local geometry is identical to that of the kagome lattice [Fig. 1(b)], the Husimi lattice has weaker geometrical frustration because of its bisimplex nature [30] and because the triangles never reconnect, giving it a tree structure. A major consequence of these features is that the Heisenberg model defined on the Husimi lattice is significantly easier to calculate than the kagome case. To be specific, the PESS Ansatz defined on the Husimi lattice is an infinite tree tensor-network state, which, as we discuss in detail in Sec. II, can be computed very efficiently by the simple-update approach [31, 32]. This allows us to perform systematic investigations within the PESS framework of the physical properties of the ground state for Heisenberg models of arbitrary spin quantum number, S, on the Husimi lattice. Within the confines of the Husimi geometry, we may thus characterize the unique quantum ground states at small S and the quantum-to-classical crossover with increasing S. Beyond the Husimi lattice, its geometrical similarity to the kagome lattice (Fig. 1) suggests the possibility of many similar physical properties [33, 34], and thus such an investigation may shed new light on the nature of the kagome system.

With this motivation, here we study the properties of the antiferromagnetic Heisenberg model on the Husimi lattice for spin quantum numbers up to $S = 4$, working directly in the theromdynamic limit by the PESS technique [16]. We find a wide variety of quantum ground states at zero field, ranging from a gapless spin liquid for $S = 1/2$ through different types of gapped, simplex-solid state for $S = 1$ and $S = 2$, to (120^0-)ordered Néel-type antiferromagnets for $S = 3/2$ and $S \geq 5/2$. Despite these differences, every single model shows a 1/3 plateau in the magnetization, suggesting a further rich variety of quantum states at finite applied fields.

This paper is organized as follows. In Sec. II, we give a brief introduction to the model and to the Husimi lattice, we review the simplex-solid states and present their generalization to situations with broken translational and spin symmetries, and we discuss the simple-update method for computations using the PESS wave function, including of the entanglement spectrum. In Sec. III, we present our results for the zero-field energies, spontaneous magnetizations, and entanglement spectra of Heisenberg models on the Husimi lattice for spin quantum numbers up to $S = 4$. In Sec. IV, we extend our considerations to a finite magnetic field, compute the induced magnetization curves for all S values, and comment in detail on the state at 1/3 of the saturation magnetization. Section V contains a discussion and a brief summary of our results.

II. MODEL AND METHOD

A. Model

We consider the nearest-neighbor antiferromagnetic Heisenberg model in the presence of an external magnetic field, h, applied in the z direction of spin space, on the Husimi lattice of Fig. 1(a). The Hamiltonian is given by

$$H = J \sum_{\langle i,j \rangle} \mathbf{S}_i \cdot \mathbf{S}_j - h \sum_i \mathbf{S}_i^z, \qquad (1)$$

where $\mathbf{S}_i$ is the spin-S operator on site i, we investigate spin quantum numbers up to $S = 4$, $\langle i, j \rangle$ denotes the sum over nearest-neighbor sites, and J is the nearest-neighbor antiferromagnetic exchange coupling, which is set henceforth as the energy scale ($J = 1$).

B. Properties of the Husimi Lattice

The Husimi tree, first introduced in statistical mechanics by Husimi [29, 35, 36], is a connected graph whose lobes are all p-polygons ($p \geq 2$, where the 2-polygon is a bond, the 3-polygon a triangle, and so on) and whose bonds belong to at most one simple cycle. If all lobes consist of only one type of p-polygon, the system is known as a pure Husimi tree, of which the simplest is the Cayley tree [37], whose lobes consist only of bonds. The Husimi lattice is an infinite pure Husimi tree. A Husimi lattice can be characterized by two numbers, p and z, where p is the number of edges of the p-polygon and z is the coordination number of each vertex. A Husimi lattice with $z = 4$ and $p > 2$ can be derived from the Bethe lattice [39] with coordination number p if each bond of the Bethe lattice is replaced by a single vertex and each vertex by a single p-polygon.

The general quasi-regular tiling $\{^p_q\}$ is composed of two types of regular polygon with edge numbers p and q, which are arranged alternately around each vertex. The coordination number of all structures $\{^p_q\}$ is equal to four. The Husimi lattice with $z = 4$ and $p > 2$ can be also regarded as a limiting case of the quasi-regular tiling $\{^p_q\}$ in the hyperbolic plane, with $q = \infty$ [38]. The $\{^3_\infty\}$ and $\{^4_\infty\}$ Husimi lattices are also known respectively as the triangular and square Husimi lattices, and in this sense the system on which we focus here is more accurately specified as the triangular Husimi lattice [Fig. 1(a)]. The kagome lattice [Fig. 1(b)] is the quasi-regular structure $\{^3_6\}$ and we stress again that the two share the same local geometry (Fig. 1).

There is, however, an essential difference between the Husimi tree and the Husimi lattice. In the same way that the Cayley tree differs from the Bethe lattice [39], the Husimi lattice has no center and no boundary, and all of its vertices (or polygons) are equivalent, thereby preserving translational invariance. By contrast, the Husimi

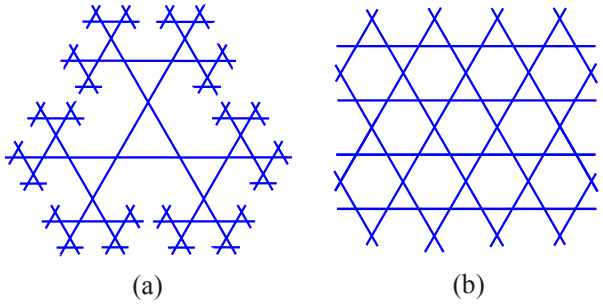

FIG. 1. (Color online) (a) Triangular Husimi lattice; (b) kagome Lattice.

tree does have a central vertex (or polygon) and a boundary; further, the number of vertices (polygons) grows exponentially with distance from the center, and thus the ratio between the number of vertices (polygons) on the boundary and that in the bulk does not approach zero in the thermodynamic limit. The Husimi tree therefore has very strong finite-size effects and the physical properties of any model defined on the finite tree may be very different from those of a model on the infinite lattice. Normally a model defined on the Husimi lattice is much more suitable to represent a real physical system than a model on the Husimi tree [39].

C. Simplex-Solid States

Here we review simplex-solid states and PESS. The simplex-solid state of an SU(N) quantum antiferromagnet was first introduced by Arovas [15] and can be regarded as a generalization of the AKLT construction [5]. In any simplex-solid state, the bond singlets of the AKLT state are extended to N-site simplex singlets. As with the AKLT state, one may construct the parent Hamiltonian, for which the simplex solid is the exact ground state, as a sum of particular local projection operators. Simplex solids typically have a gap to all excitations and short-ranged correlation functions.

PESS were introduced by Xie *et al.* [16], by generalizing the concept of simplex-solid states to a numerical Ansatz designed to solve the $S = 1/2$ kagome Heisenberg antiferromagnet. PESS are also an extension of PEPS [40], sharing a number of the advantages of the PEPS formulation, including the ability to satisfy the boundary area law of entanglement entropy and to represent any state if the bond dimension is sufficiently large. Beyond the PEPS framework, PESS introduce a new type of entangled simplex tensor, which captures the N-body entanglement of the N virtual particles within an N-site simplex (beyond the 2-body entanglement contained in PEPS), and it is believed that this feature has an essential role in reproducing the properties of frustrated systems [16].

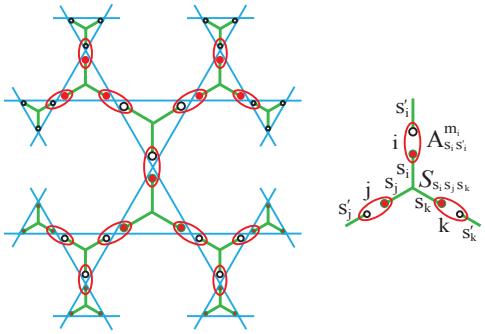

FIG. 2. (Color online) PESS representation of a simplex-solid state on the infinite Husimi lattice. Solid circles represent virtual spins $S = n$, open circles virtual spins $S = n - 1$ (n) for a $S = 2n - 1$ ($S = 2n$) simplex-solid state. Red ellipses represent the projection tensors, $A^{m_i}_{s_i s'_i}$, which project the two virtual spins into the physical spin subspace. $S_{s_i s_j s_k}$ denotes the simplex tensor, defined on every triangular unit.

PESS are precisely the tensor-network representation of the simplex-solid states [16]. Taking the example of the spin-2 simplex-solid state on the (triangular) Husimi lattice, the physical $S = 2$ spin at each site can be treated as a symmetric superposition of two virtual $S = 1$ spins. Because of the bisimplex property, meaning that two neighboring simplices share a single site symmetrically, each of the $S = 1$ spins can be assigned to one of the simplices. Thus each simplex contains three virtual $S = 1$ spins. From the properties of the SU(2) group, decomposition of the product of three integer spins yields

$$n \otimes n \otimes n = [a_0 \times 0] \oplus \cdots \oplus [a_k \times k] \oplus \cdots \oplus [a_{3n} \times 3n],$$
$$a_k = \begin{cases} 2k+1, & k \le n \\ 3n+1-k, & k > n \end{cases}, \quad k = 0, 1, \ldots, 3n, \tag{2}$$

where a_k represents the number of times that the kth irreducible representation occurs. a_0 is always equal to 1, i.e. the three-site simplex contains a unique spin singlet state. One may thus define a virtual singlet on each simplex,

$$|\psi_\alpha\rangle = \frac{1}{\sqrt{6}} \sum_{\{s \in \alpha\}} S^{\alpha}_{s_i s_j s_k} |s_i, s_j, s_k\rangle, \tag{3}$$

where s_i is a $S = 1$ virtual spin located at site i belonging to the simplex α, and $S^{\alpha}_{s_i s_j s_k}$ is an antisymmetric Levi-Civita tensor, $\epsilon_{s_i s_j s_k}$. Recovery of the physical spin-2 state requires the application of a mapping P_i at each site i, which projects the two virtual $S = 1$ spins into the spin-2 subspace,

$$P_i = \sum_{s_i, s'_i} \sum_{m_i} A^{m_i}_{s_i, s'_i} |m_i\rangle\langle s_i, s'_i|, \tag{4}$$

where $|m_i\rangle$, with $m_i = 0, \pm 1, \pm 2$, is a basis state of the physical $S = 2$ spin at site i. $A^{m_i}_{s_i, s'_i}$ is the Clebsch-Gordan

coefficient symmetrizing two virtual $S = 1$ spins and has nonvanishing components $A^{2}_{11} = A^{-2}_{33} = 1$, $A^{1}_{12} = A^{1}_{21} = A^{-1}_{23} = A^{-1}_{32} = 1/\sqrt{2}$, $A^{0}_{13} = A^{0}_{31} = 1/\sqrt{6}$, and $A^{0}_{22} = 2/\sqrt{6}$ [16]. Finally, the tensor-network representation of this simplex-solid state is the PESS

$$|\Psi\rangle = \bigoplus_i P_i \prod_\alpha |\psi_\alpha\rangle \qquad (5)$$
$$= \mathrm{Tr}(...S^{\alpha}_{s_i s_j s_k} A^{m_i}_{s_i,s_i'} A^{m_j}_{s_j,s_j'} A^{m_k}_{s_k,s_k'} ...)|...m_i m_j m_k...\rangle.$$

This description can be extended to any higher even-integer spin. A physical $S = 2n$ spin is regarded as a symmetric superposition of two virtual $S = n$ spins and the three spins in each simplex are combined to form an SU(2) simplex singlet. By covering the lattice with equivalent simplex singlets, one obtains a class of simplex-solid states breaking no lattice symmetries. Their parent Hamiltonians are readily constructed in terms of local projection operators. Because half of the virtual spins at the three vertices of any given simplex are combined into a singlet ($S = 0$), the total spin on each simplex cannot exceed $S = 3n$. The uniform simplex-solid states are therefore the exact ground state of the Hamiltonian

$$H = \sum_{m=3n+1}^{6n} J_m \sum_{\langle ijk\rangle \in \triangle,\nabla} P_m(ijk) \qquad (6)$$

where the second sum $\langle ijk\rangle$ is over all simplices ($\triangle$ and ∇), J_m represents a set of non-negative coupling constants, and $2n$ ($= S$) is the physical spin quantum number at each site. $P_m(ijk)$ is the operator projecting a state at each simplex onto a state with total spin m, which can be expressed as

$$P_m(ijk) = \prod_{l\neq m}^{3S} \frac{(\mathbf{S}_i + \mathbf{S}_j + \mathbf{S}_k)^2 - l(l+1)}{m(m+1) - l(l+1)}, \qquad (7)$$

where $\mathbf{S}_i$, $\mathbf{S}_j$, and $\mathbf{S}_k$ are the vector spin operators on the three sites of every simplex.

D. PESS States with Broken Symmetry

1. *Broken Translational Symmetry*

To extend the discussion of the previous subsection to systems with arbitrary odd-integer spin, a physical $S = 2n-1$ spin must be regarded as a symmetric superposition of a virtual $S = n$ spin and a virtual $S = n-1$ spin. One possible distribution of these unequal spins is to assign the $S = n$ spins to one type of simplex, for example the upward-oriented triangles (Δ, referred to henceforth as "up-triangle"), and the $S = n-1$ spins to the other (∇, henceforth "down-triangle"). Following Eq. (2), the three $S = n$ spins on the up-triangles combine to form an SU(2) spin singlet, and so do the three $S = n-1$ spins on the down-triangles. A non-uniform simplex-solid state can be obtained by arranging the two inequivalent types of simplex singlet in an alternating pattern on the Husimi lattice, with the inequivalence causing a two-fold ground-state degeneracy. This class of simplex-solid states breaks lattice inversion symmetry and favors trimerization [25]. Because the total spin of the three sites on each bond pair $\langle$, spanning every pair of inequivalent simplices, cannot exceed $2S$, these simplex-solid states are exact zero-energy eigenstates of the parent Hamiltonian [15]

$$H = \sum_{m=2S+1}^{3S} J_m \sum_{\langle ijk\rangle \in \langle} P_m(ijk), \qquad (8)$$

where the second sum $\langle ijk\rangle$ is over all three-site trios (ijk) defining one bond on each type of simplex, J_m is a set of non-negative coupling constants, S is the physical (site) spin quantum number, and $P_m(ijk)$ is the spin projection operator defined by Eq. (7), but with the three sites specified to be on the same trio $\langle$.

The simplest example of a non-uniform simplex-solid state is obtained for $S = 1$. This is readily expressed as a PESS wavefunction with bond dimension $D = 4$, where the two virtual spins at every lattice site each have four basis states, $|1\rangle \equiv |\uparrow\rangle$, $|2\rangle \equiv |0\rangle$, $|3\rangle \equiv |\downarrow\rangle$, and $|4\rangle \equiv |\emptyset\rangle$, representing respectively the components of a spin-1 triplet and a spin-0 net singlet. The nonvanishing components of the two simplex tensors are $S^{\triangle}_{ijk} = \frac{1}{\sqrt{6}}\epsilon_{ijk}$ ($i,j,k = 1,2,3$) and $S^{\nabla}_{444} = 1$, and of the projection tensor are $A^{+1}_{14} = A^{0}_{24} = A^{-1}_{34} = A^{+1}_{41} = A^{0}_{42} = A^{-1}_{43} = 1$, $A^{+1}_{12} = A^{0}_{13} = A^{-1}_{23} = 1/\sqrt{2}$, and $A^{+1}_{21} = A^{0}_{31} = A^{-1}_{32} = -1/\sqrt{2}$; the parent Hamiltonian is given simply by

$$H = \sum_{\langle ijk\rangle \in \langle} P_3(ijk). \qquad (9)$$

We comment that there is no corresponding simplex-solid state on the triangular Husimi or kagome lattice for the case when the spin quantum number is half-odd-integer. In this situation, and indeed for any other with an odd-site simplex, decomposing the product of an odd number of half-odd-integer spins cannot yield a total spin singlet.

2. *Spontaneously Broken Spin Symmetry*

In two and higher dimensions, and in particular as the spin quantum number increases, the ground state of any magnetic system usually favors some type of ordered state. For strongly frustrated antiferromagnets, where collinear order is precluded, this order tends to be coplanar in the absence of an external field, and in triangle-based geometries its most common form is the 120-degree Néel order shown in Fig. 3(a). To detect this type of magnetic order in our PESS calculations, one could in principle calculate the expectation values of the

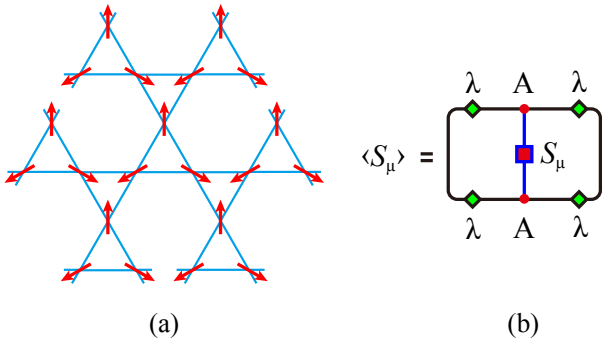

FIG. 3. (Color online) (a) Schematic representation of the antiferromagnetic state with 120-degree Néel order on the Husimi lattice, where the arrows denote the orientations of the spins. (b) Graphical representation of the expectation value of the local spin operator, $S_\mu(\mu = x, y, z)$, for a PESS wave function, where λ and A are respectively the bond vector and the projection tensor in the canonical PESS wave function. Connecting lines denote the contraction of two neighboring tensors.

spin operators at every site and then consider their mutual orientations. For the 3-PESS wave function used in this work [16], we assume complete translational invariance and thus we need only calculate the expectation values of the spin operators $\langle S_i^x\rangle$, $\langle S_i^y\rangle$, and $\langle S_i^z\rangle$ at the three sites within each of the two types of triangle (up and down). Because the PESS wavefunction defined on the Husimi lattice can be expressed in canonical form, as shown in next subsection, the expectation value of the local spin operator is easy to calculate, as represented graphically in Fig. 3(b). If the ground state has antiferromagnetic order, the ("transverse") magnetization,

$$M = \frac{1}{N}\sum_i \sqrt{\langle S_i^x\rangle^2 + \langle S_i^y\rangle^2 + \langle S_i^z\rangle^2}, \qquad (10)$$

will have a finite value. The spontaneous magnetization M serves as the order parameter for the detection of antiferromagnetically ordered states.

3. *Applied Magnetic Field*

In the presence of a finite field, h, in Eq. (1), spin rotation symmetry is broken explicitly. In this case it is the longitudinal magnetization, defined as

$$M_z = \frac{1}{N}\sum_i \langle S_i^z\rangle, \qquad (11)$$

which takes on a finite value. In contrast to numerical approaches implemented on systems of finite size, where it is necessary to target sectors of specific total-spin quantum number to reproduce the effects of an external field,

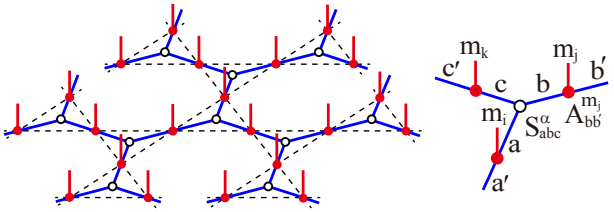

FIG. 4. (Color online) Graphical representation of a PESS on the infinite Husimi lattice (dashed lines). Open black circles represent the three-index simplex tensor, S^α_{abc} ($\alpha = \triangle, \nabla$), solid red circles the three-index projection tensors, $A^{m_j}_{bb'}$, at each physical lattice site. Blue lines represent the virtual indices of all tensors, vertical red lines the physical degrees of freedom, $\{m_j\}$, of each site.

tensor-network techniques are already in the thermodynamic limit and will return a wave function appropriate for the field applied. We calculate the longitudinal magnetization associated with this wave function for all values of h and S in Sec. IV, and interpret the physical content of the resulting states.

We comment here that the PESS code we use in this paper is real. Thus it is possible to represent all magnetic states where the spins are coplanar, which naturally includes all collinear spin states. In the event that the combination of frustration and applied magnetic field were to produce non-coplanar spin states, or in field-free systems with extended frustration showing, for example, the double-spiral ground state, it would be necessary to use complex code to obtain an accurate representation. In the present case, with nearest-neighbor coupling only and triangular geometries, it is expected [41] that the moments will lie in the same plane for all applied fields.

E. Simple-Update Method and Canonical Form

We now employ the PESS wave function not as an exact description of simplex-solid states but as a variational Ansatz to capture the ground-state properties of an arbitrary spin system [16]. The PESS wave function on the triangular Husimi lattice is represented graphically in Fig. 4. Known as a 3-PESS because its simplex contains three lattice sites, it is composed of simplex entanglement tensors and projection tensors. The former, $S^\triangle_{abc}$ and S^∇_{abc}, each have three virtual indices and form a Bethe lattice of simplex triangles, while the latter, $A^m_{aa'}$, $A^m_{bb'}$, and $A^m_{cc'}$, each have one physical and two virtual indices and are located at the decorating sites of this Bethe lattice (the original sites of the Husimi lattice). In contrast to Sec. IIC, where the tensor indices for the simplex solid were virtual spin indices, now a, a', b, ... are general virtual indices of the tensor network and their dimension is the bond dimension, D. Each physical index, m_i, runs over the $d = 2S + 1$ physical basis states defined on each lattice site, i.

The ground-state wave function is obtained by repeated application of imaginary-time evolution operators, $U(\tau) = \exp(-\tau H)$, on an initial PESS wavefunction, $|\Psi_0\rangle$, where τ is taken to be small. The Hamiltonian is split into

$$H = H_{\triangle} + H_{\nabla}, \tag{12}$$

where $H_{\triangle}$ and H_{∇} contain respectively the Hamiltonian terms on all up- and down-triangles. Because $H_{\triangle}$ and H_{∇} do not commute, the evolution operator is decomposed approximately into a product of two near-unitary operators using the Trotter-Suzuki formula,

$$e^{-\tau H} = e^{-\tau H_{\triangle}} e^{-\tau H_{\nabla}} + O(\tau^2). \tag{13}$$

Each iteration of the projection is then performed in two steps by successive application of $e^{-\tau H_{\triangle}}$ and $e^{-\tau H_{\nabla}}$ to the wave function.

Each projection step, or application of $e^{-\tau H_\alpha}$ to the wave function ($\alpha = \triangle, \nabla$), increases the dimensions of the evolved bonds and thus requires a truncation of the bond dimensions of the new tensors. During this truncation, it is necessary to consider the renormalization effect of all the other bonds of the system, which can be encoded as environment tensors, and in general there are two types of scheme to simulate their contributions. In the full-update approach, a complete and accurate environment tensor is calculated at each projection step, but the rather high computational cost of this process limits the bond dimension to very small values (approximately $D \leq 6$). A more efficient approach, the simple-update method [16, 31, 42, 43], approximates the effect of the environment tensor using specific positive bond vectors. This method turns out to be almost exact for one-dimensional systems [44] and, of key importance for the present study, for systems defined on the Bethe lattice [32], as long as the imaginary time step τ is taken to be sufficiently small.

The reason for this result lies in the bipartite nature of tensor-network states defined on open chains and on the Bethe lattice. This allows them to be written in canonical form (below) and divided into two subsystems under Schmidt decomposition [45], such that the square of the bond vector defined on each bond is precisely the eigenvalue of the reduced density matrix if the tensor-network state is kept in its canonical form [32, 44]. The bond vector then contains all entanglement information between the system and environment subblocks, making the simple-update method equivalent to the full-update approach for bipartite tensor-network states. Because PESS defined on the Husimi lattice are also bipartite tree tensor-network states, one expects that the simple-update approach will provide an efficient determination of the wave function in this case.

The simple-update procedure for the PESS wave function is specified by the following steps, represented graphically in Fig. 5.

(i) Absorb the environment bond vectors $\lambda_{\beta,v}$ into the projection tensors $A^m_{vv'}$ and then contract the three projection tensors with the simplex tensor S^α to obtain a cluster tensor T^α, where $v = a, b, c$ represents the virtual bond index, m is the physical index of the projection tensor, and α and β denote two neighboring simplices (up- or down-triangles).

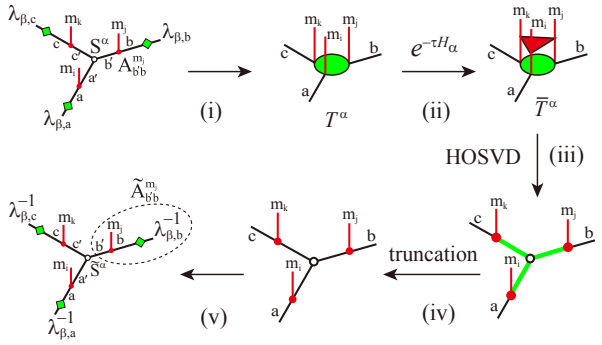

FIG. 5. (Color online) Graphical representation of the simple-update procedure for PESS using HOSVD. Details are provided in the text.

(ii) Apply the near-unitary evolution operator $e^{-\tau H_\alpha}$ to the cluster tensor T^α to obtain a new cluster tensor $\bar{T}^\alpha$.

(iii) Decompose the new cluster tensor $\bar{T}^\alpha$ into the product of a renormalized simplex tensor and three renormalized projection tensors by using higher-order singular value decomposition (HOSVD) [16, 46, 47]. At the same time, one obtains the new bond vectors $\tilde{\lambda}_{\alpha,v}$.

(iv) Truncate the renormalized simplex tensor and the three renormalized projection tensors to obtain the updated simplex tensor $\tilde{S}^\alpha$ and projection tensors.

(v) Absorb the inverse bond vectors $\lambda^{-1}_{\beta,v}$ into the truncated projection tensors to obtain the updated projection tensors $\tilde{A}^m_{vv'}$.

One evolution cycle is completed, i.e. the full tensor network is updated, by repeating this procedure for each simplex ($\alpha = \triangle, \nabla$). Repeated update cycles cause the PESS wave function to converge to the ground state.

The canonical PESS wave function on the Husimi lattice can be obtained by the simple-update method if the evolution operator is replaced by the identity operator in step (ii). In the canonical form, all tensors of the PESS should simultaneously satisfy the canonical conditions

$$\begin{aligned}
\sum_{a,b} S^\alpha_{abc} (S^\alpha_{abc'})^* &= \delta_{c,c'} \lambda^2_{\alpha,c}, \\
\sum_{v,m} \lambda^2_{\alpha,v} A^m_{vv'} (A^m_{vv''})^* &= \delta_{v',v''}, \\
\sum_{v,m} \lambda^2_{\alpha,v} A^m_{v'v} (A^m_{v''v})^* &= \delta_{v',v''},
\end{aligned} \tag{14}$$

where $\lambda_{\alpha,v}$ denotes the bond vector for the bond linking the S^α and $A^m_{vv'}$ tensors; the "left" and "right" conditions specified in the lower two lines must both be satisfied separately. Maintaining this canonical form is the key to

the success of the simple-update scheme and is possible due to the bipartite nature of the system.

F. Entanglement spectrum

The entanglement spectrum (ES) of a quantum system is defined as the logarithmic eigenvalue of the reduced density matrix of a many-body state [48], and provides additional useful information beyond the entanglement entropy [24, 48, 49]. As noted above, for a canonical tensor-network state, the square of the bond vector is precisely the eigenvalue of the reduced density matrix, and thus it is easy to calculate the ES using the bond vectors,

$$\zeta_\alpha(i) = -\mathrm{Log}_2\, \lambda^2_{\alpha,v}(i), \quad i = 1, 2, 3, \ldots, D, \tag{15}$$

where $\lambda_{\alpha,v}$ satisfies the normalization condition $\sum_i \lambda^2_{\alpha,v}(i) = 1$.

Taking the $S = 2$ simplex-solid state on the Husimi lattice as an example, its tensor-network representation is a PESS wave function with bond dimension $D = 3$, as shown in Subsec. II C. All the bond vectors obtained from the canonical form [Eq. (15)] are $\lambda_{\alpha,v} = (1, 1, 1)/\sqrt{3}$, which is the square root of the reduced density matrix associated with a simplex-singlet state [Eq. (3)]. Specifically, $\hat{\rho}_s = tr_E(\hat{\rho}) = \sum_{s_i,s_i'}(\frac{1}{6}\sum_{s_j,s_k}\epsilon_{s_i s_j s_k}\epsilon_{s_i' s_j s_k})|s_i'\rangle\langle s_i| = \sum_{s_i,s_i'}(\frac{1}{3}\delta_{s_i,s_i'})|s_i'\rangle\langle s_i|$. This result states that, if there exists a total singlet on the triangular simplex, then the ES on the corresponding bond will be three-fold degenerate. For the $S = 2$ simplex-solid state, because there is a total singlet on every simplex, the ES is three-fold degenerate on every bond of the system. Further, the energy of this simplex-solid state for the Heisenberg model on the Husimi lattice is given exactly as $E_0 = -9/2$, and there is no magnetic order.

It is similarly straightforward to obtain the ES of the $S = 1$ simplex-solid state on the Husimi lattice, whose tensor-network representation is a PESS wave function with bond dimension $D = 4$, as shown in Subsec. II C. For convenience of discussion, henceforth we use the terminology "A-bond" ("B-bond") to denote the bond linking the $S^{\triangle}_{abc}$ (S^{∇}_{abc}) and $A^m_{vv'}$ tensors. After this wave function is put in canonical form, the bond vectors on the A- and B-bonds are $(1, 1, 1, 0)/\sqrt{3}$ and $(1, 0, 0, 0)$, indicating that their entanglement spectra are respectively three- and one-fold degenerate (i.e. non-degenerate), as could be expected from the preceding analysis. If the energy of this state is computed, one indeed finds strong trimerization "order" characterized by $\Delta E = 2|E_{\triangle} - E_{\nabla}|/3 = 2$, where $E_{\triangle}$ (E_{∇}) is the average energy of an up-triangle (down-triangle), but no magnetic order.

As for the AKLT states, the degeneracy of the ES for simplex-solid states may be understood from the viewpoint of edge states [45]. We first consider the edge states of the odd-integer-spin simplex-solid state, with

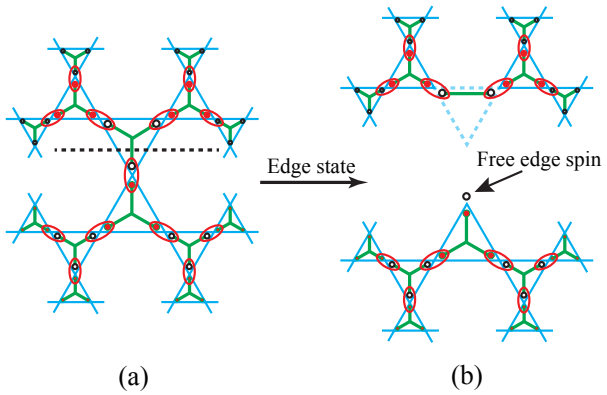

FIG. 6. (Color online) Schematic representation of (a) a simplex-solid state and (b) the corresponding edge state. Solid red circles denote virtual spins $S = n$ and open black circles virtual spins $S = n - 1$ ($S = n$) for odd-integer-spin simplex-solid states (even-integer-spin simplex-solid states). The edge state can be obtained by cutting a single bond of the PESS and has a free edge spin on its boundary.

$S = 2n - 1$, defined on the Husimi lattice. As shown in Fig. 6(a), cutting an A-bond of the PESS creates a free virtual spin $S = n$ at the boundary, represented in Fig. 6(b). Thus the edge state has a $(2n+1)$-fold degeneracy, which is related directly to the $(2n+1)$-fold degeneracy of the lowest level of the corresponding ES (three-fold degeneracy for the $S = 1$ simplex-solid state). Similarly, cutting a B-bond creates a free virtual spin $S = n - 1$ at the boundary, which is related to the $(2n - 1)$-fold degeneracy of the lowest level of its corresponding ES (non-degenerate for $S = 1$).

By contrast, for a $S = 2n$ simplex-solid state, the free virtual spin obtained at the boundary by cutting any bond is $S = n$, giving a $(2n + 1)$-fold degenerate edge state in every case and corresponding to the $(2n + 1)$-fold degeneracy of the lowest levels of the ES on both A- and B-bonds. This analysis is fully consistent with the above results for $S = 2$ simplex-solid state. We have also verified numerically that the ES of the exact $S = 3$ and $S = 4$ simplex-solid states confirm this reasoning; in the $S = 3$ case we find that the lowest levels of the ES for the A- and B-bonds are respectively five- and three-fold degenerate, while for $S = 4$ both are five-fold degenerate.

III. GROUND STATES AT ZERO FIELD

A. $S = 1/2$

We begin our presentation of PESS results for the Heisenberg model on the Husimi lattice by considering spin quantum number $S = 1/2$. This model was studied recently by Liu *et al.* [50], who concluded that its ground state was a featureless quantum spin liquid, with no local magnetization [Eq. (10)] and no gap, but with expo-

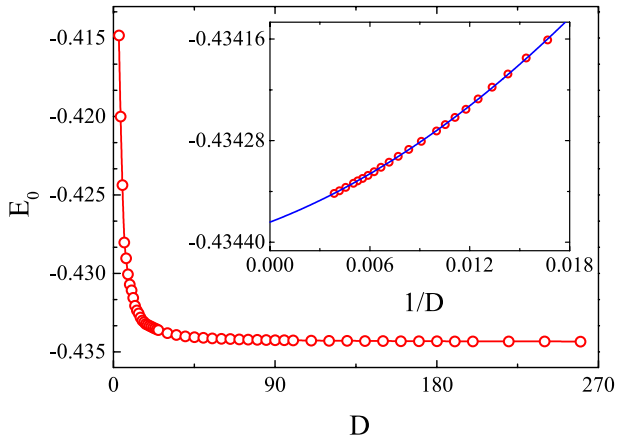

FIG. 7. (Color online) Energy per site, E_0, of the $S = 1/2$ Heisenberg model as a function of bond dimension, D. The inset shows the energy as a function of $1/D$, with a polynomial fit shown in blue. The extrapolated energy is $E_0^\infty = -0.43438(1)$.

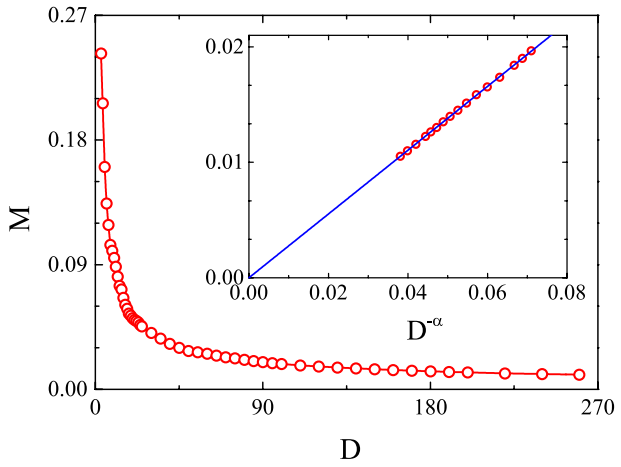

FIG. 8. (Color online) Local magnetization, M, of the $S = 1/2$ Heisenberg model as a function of bond dimension, D. The inset shows M as a function of $D^{-\alpha}$, with $\alpha = 0.588(2)$. The intercept of the linear fit (solid blue line) is $M(\infty) = 0.00000(4)$.

nentially decaying spin-spin and dimer-dimer correlation functions (these results are mutually consistent due to the special properties of infinite Bethe-type lattices, of which the Husimi lattice is an example [32]). However, we note that the correlation functions and magnetization were calculated by these authors at finite temperature ($T/J = 0.01$), and thus their results could be understood simply from the Mermin-Wagner Theorem [51], which states that there can be no spontaneously broken continuous spin symmetry at finite temperatures in one and two dimensions.

Here we investigate the properties of the model at zero temperature and perform careful extrapolations to the limit of infinite bond dimension, D. The ground-state energy per site, $E_0(D)$, is shown in Fig. 7 for values up to $D = 260$; its extrapolation to infinite D (inset, Fig. 7), obtained by a quadratic fit, is $E_0^\infty = -0.43438(1)$, and thus agrees within the error bars with the result of Ref. [50]. If we consider the magnetization order parameter, M (10), shown in Fig. 8, we find that this is finite at every value of D, but decreases as D increases. We also confirm that the spin orientations conform to the expected 120-degree Néel order (Fig. 3) and that the spin magnitudes, $\sqrt{\langle S_i^x\rangle^2 + \langle S_i^y\rangle^2 + \langle S_i^z\rangle^2}$, are identical at every site within numerical error.

The key question is how this magnetization behaves in the limit of infinite D. On logarithmic axes, our $M(D)$ data from $D = 90$ to 260 fall on a perfectly straight line, whose gradient we obtain as $\alpha = -0.588(2)$. The inset of Fig. 8 shows this purely algebraic functional form, $M \propto D^{-\alpha}$. We do not show data for spin-spin or dimer-dimer correlation functions because, as noted above, they contain no new information about the gapped or gapless nature of the system. The key issue is instead the question of whether the gapless, algebraic system may in fact have long-range magnetic order. Extrapolation of our results to the limit $D \to \infty$ yields the result $M(\infty) = 0.00000(4)$. To summarize, we have taken extreme care to obtain the most precise, high-D data at zero temperature and to extrapolate it following the most accurate possible protocols, which leads us to conclude that the ordered moment vanishes, and does so algebraically. Taking this result in combination with the polynomial convergence of the ground-state energy (Fig. 7), we therefore draw one of the most important conclusions of the present study, that the true ground state of the $S = 1/2$ Heisenberg model on the triangular Husimi lattice is a gapless, non-magnetic state, i.e. an algebraic spin liquid.

For completeness we show in Fig. 9 the ES of the $S = 1/2$ Heisenberg model on the Husimi lattice. Clearly all levels of the ES are non-degenerate, with the lowest three well separated from the others. We return below to an interpretation of these results in the light of our further findings.

B. $S = 1$

Turning to the $S = 1$ Heisenberg model on the Husimi lattice, in Fig. 10 we present our results for the ground-state energy per site, E_0, up to $D = 100$. Once again E_0 decreases monotonically with D, converging rapidly (inset, Fig. 10) to $E_0 = -1.405861(1)$ in the infinite-D limit. However, significantly more insight into the nature of the ground state may be obtained from the energy difference between between up- and down-triangles, $\Delta E = 2|E_\triangle - E_\triangledown|/3$, which we show as a function of D in Fig. 11. ΔE may be considered as a type of trimerization "order parameter," and undergoes a rapid onset at $D = 8$. The magnetic order parameter, M, also shown

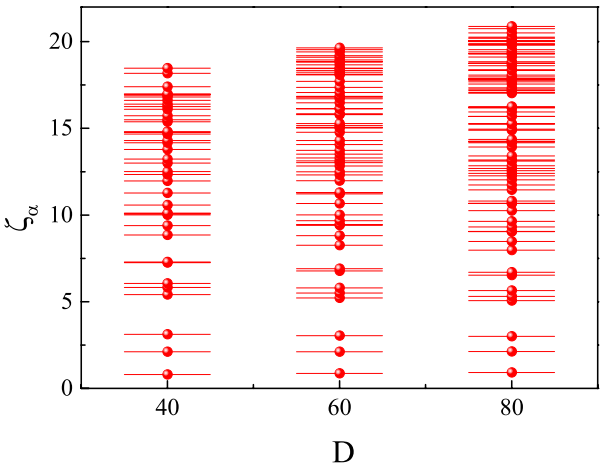

FIG. 9. (Color online) Entanglement spectra of the $S = 1/2$ Heisenberg model with $D = 40$, 60, and 80. The number of dots on each level denotes its degeneracy; every low-lying level in the spectrum is non-degenerate.

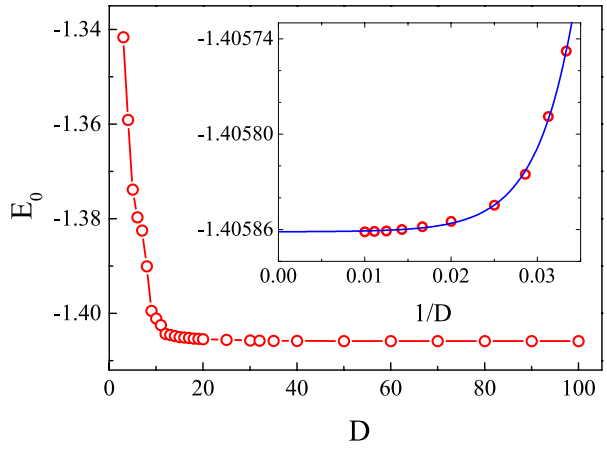

FIG. 10. (Color online) Energy per site, E_0, of the $S = 1$ Heisenberg model as a function of bond dimension, D. The inset shows the energy as a function of $1/D$, with an exponential fit shown in blue. The extrapolated energy is $E_0^\infty = -1.40586(1)$.

in Fig. 11, undergoes an equally rapid fall to zero at the same value, while the correlation length (inset, Fig. 11) also drops abruptly. These features all demonstrate that a phase transition from a magnetically ordered state to a nonmagnetic, trimerized state occurs at the bond dimension $D_c = 8$, which we note corresponds to the minimum D required to describe a state of finite trimerization.

The energy difference, ΔE, converges to a constant value [0.29021(1)] as D becomes large, indicating that the trimerized state persists as the true ground state. To confirm this result, we calculated the ES of the $S = 1$ model, which is shown in Fig. 12. Clearly the lowest-lying level on the A-bond is three-fold degenerate while that

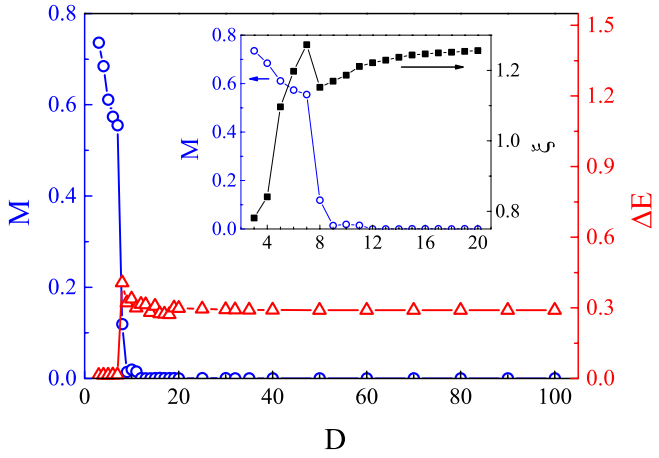

FIG. 11. (Color online) Trimerization parameter $\Delta E = 2|E_\triangle - E_\triangledown|/3$ (open red triangles), where $E_{\triangle(\triangledown)}$ is the average energy of an up-triangle (down-triangle), and local magnetization, M (open blue circles), both shown as a function of bond dimension, D. Finite trimerization and vanishing magnetization occur simultaneously when $D \geq 8$. The correlation length, ξ (solid black squares), also drops abruptly at $D = 8$, as shown in the inset, further confirming the occurrence of a phase transition at the bond dimension $D_c = 8$. The trimerization converges to a constant value, $\Delta E = 0.29021(1)$, at large D.

on the B-bond is non-degenerate. These are exactly the properties of the non-uniform simplex solid state of the $S = 1$ model discussed in Subsec. II F. Thus the ES verifies that the ground state of the $S = 1$ Heisenberg model on the Husimi lattice is a trimerized simplex-solid state with a spontaneous breaking of lattice inversion symmetry. The most direct demonstration that this state has a finite gap is obtained from the longitudinal magnetization (Sec. IID3), which we discuss in detail in Sec. IV.

As noted in Sec. I, the $S = 1$ Heisenberg model on the kagome lattice has recently attracted strong attention. Older proposals for the ground state, including the hexagonal singlet solid [22] and the resonating AKLT loop state [23, 24], appear to have been supplanted by a trimerized simplex-solid state [25–27], which has the best variational energy, $E_0^k = -1.4116(4)$ [26]. This is a symmetry-broken state with trimerization order, which as above can be defined by the difference of the average energies between up- and down-triangle simplices, quoted in Ref. [26] as 0.261, or approximately 19% of E_0^k. Here we have shown that the same model on the Husimi lattice has exactly the same type of ground state, a trimerized simplex solid, with a remarkably similar energy, $E_0 = -1.40586$, and a trimerization parameter of approximately 20.6%. Thus one may conclude that the vast majority of energetic effects on the two lattices are dominated by extremely local processes.

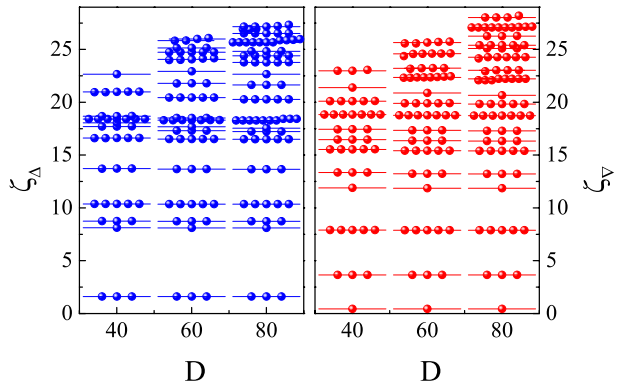

FIG. 12. (Color online) Entanglement spectra of the $S = 1$ Heisenberg model with $D = 40$, 60, and 80 on A-bonds (left) and B-bonds (right). The number of dots on each level denotes its degeneracy. Three-fold degeneracy of the lowest A-bond levels indicates simplex singlet entanglement within the up-triangles, whereas the non-degenerate B-bond levels indicate its absence within the down-triangles.

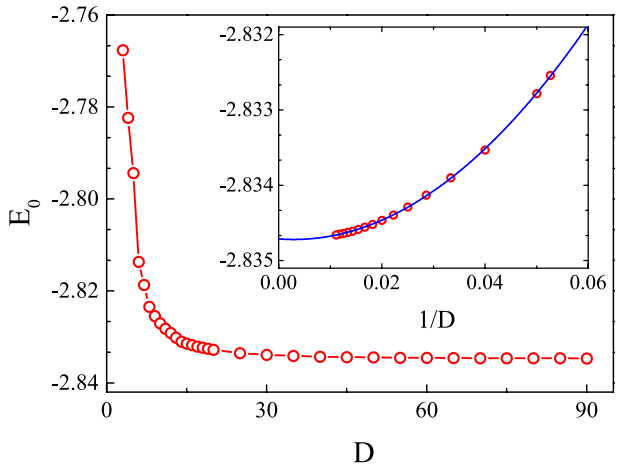

FIG. 13. (Color online) Energy per site, E_0, of the $S = 3/2$ Heisenberg model as a function of bond dimension, D. The inset shows the energy as a function of $1/D$, with a polynomial fit shown in blue. The extrapolated energy is $E_0^\infty = -2.83471(1)$.

C. $S = 3/2$

For the $S = 3/2$ case, we find as for $S = 1/2$ that the ground-state energy per site converges algebraically [to $E_0^\infty = -2.83471(1)$] with increasing bond dimension, as shown in Fig. 13; such convergence behavior indicates that the system is gapless. However, the magnetic order parameter, shown in Fig. 14, converges not to zero at large D but to a finite value, $M(\infty) = 0.856(3)$. This robust magnetization is approximately 57% of the classical value for an $S = 3/2$ system. Néel order is of course consistent with gapless excitations and algebraic convergence of $E(D)$, but demonstrates clearly that the physics

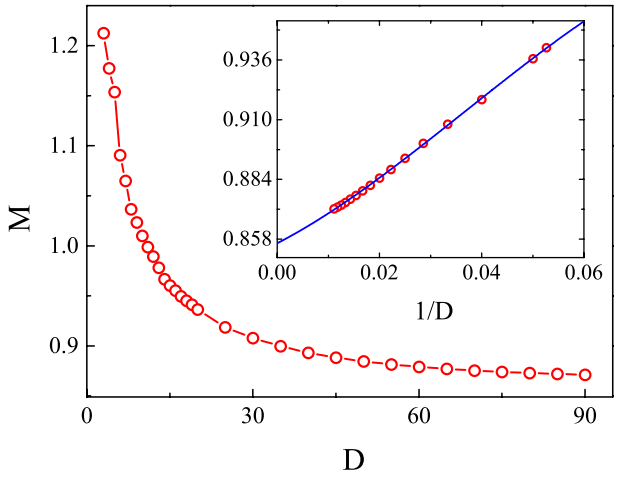

FIG. 14. (Color online) Local magnetization, M, of the $S = 3/2$ Heisenberg model as a function of bond dimension, D. The inset shows M as a function of $1/D$, with a polynomial fit shown in blue. The extrapolated M has a finite value at infinite D, $M(\infty) = 0.856(3)$.

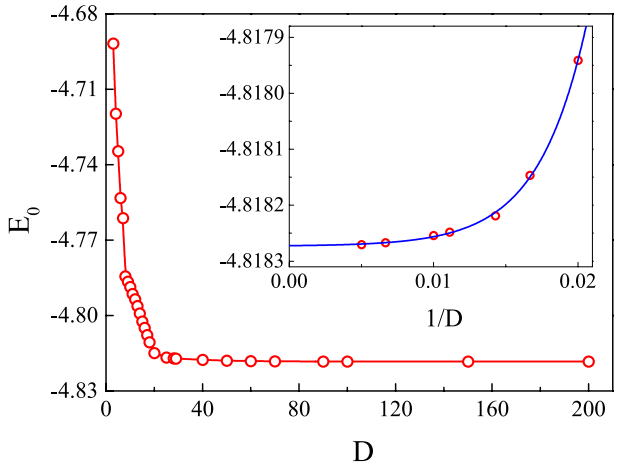

FIG. 15. (Color online) Energy per site, E_0, of the $S = 2$ Heisenberg model as a function of bond dimension, D. The inset shows the energy as a function of $1/D$, with as exponential fit shown in blue. The extrapolated energy is $E_0^\infty = -4.8185(4)$.

of the $S = 3/2$ Husimi lattice has more in common with high-dimensional antiferromagnets than with the physics of spin chains and the Haldane conjecture. We defer a discussion of the ES for this case to Sec. IIIE.

D. $S = 2$

Turning to the Heisenberg model with $S = 2$, the ground-state energy per site (Fig. 15) again converges monotonically and rapidly to $E_0^\infty = -4.8185(4)$; as for

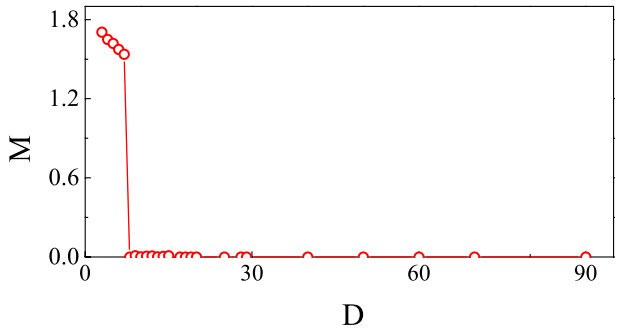

FIG. 16. (Color online) Local magnetization, M, of the $S = 2$ Heisenberg model as a function of bond dimension, D. Sudden vanishing of M for bond dimension $D \geq 8$ indicates a transition to a non-magnetic state.

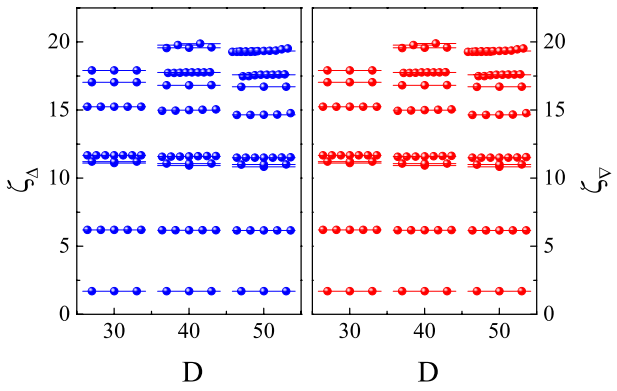

FIG. 17. (Color online) Entanglement spectra of the $S = 2$ Heisenberg model with $D = 30$, 40, and 50 on A-bonds (left) and B-bonds (right). The number of dots on each level denotes its degeneracy. Three-fold degeneracy of the lowest-lying levels for every bond in the system indicates singlet entanglement within every simplex (triangle).

$S = 1$, we fit only the higher-D values of this somewhat stepwise convergence to an exponential form. Also as for $S = 1$, we find again that the magnetization, M, vanishes suddenly for $D \geq 8$, as shown in Fig. 16, proving that the ground state in this case is non-magnetic. For a direct calculation of the spin gap, the longitudinal magnetization (Sec. IID3) is shown in Sec. IV.

Further insight into the nature of this spin liquid is obtained from the ES, shown in Fig. 17. Unlike the $S = 1$ case, here the lowest levels on both A- and B-bonds are three-fold degenerate, demonstrating the presence of a simplex singlet on every simplex in the system. These results are fully consistent with those obtained for the exact $S = 2$ simplex-solid state discussed in Subsec. II F, and thus the ES indicates that the ground state for $S = 2$ is a uniform simplex-solid state.

For further confirmation of the properties of this simplex solid, we calculate the expectation value of the spin projection operator, P_J^α [Eq. (7)], which projects the state at each simplex α onto a state of total spin J. From the values given in Table I, it is clear that the quantity $\langle\Psi|P_0^\alpha + P_1^\alpha + P_2^\alpha + P_3^\alpha|\Psi\rangle = 0.9947(1)$ is very close to unity, i.e. it is very improbable that the total spin at each simplex could exceed 3. Following the analysis of Sec. II C, there is therefore a simplex singlet [which belongs to the $S = 0$ subspace of $(1\otimes1\otimes1)$] on every simplex with near-unit probability. Thus the ground state of the $S = 2$ Heisenberg model on the Husimi lattice lies very close to the exact simplex-solid state.

TABLE I. Expected values of spin projection operators at each simplex for the $S = 2$ Heisenberg model on the Husimi lattice, calculated with bond dimension $D = 40$.

	$\langle\Psi\|P_J^\triangle\|\Psi\rangle$	$\langle\Psi\|P_J^\nabla\|\Psi\rangle$
$J = 0$	0.1189(1)	0.1189(1)
$J = 1$	0.5391(1)	0.5391(1)
$J = 2$	0.2803(1)	0.2803(1)
$J = 3$	0.0564(1)	0.0564(1)
$J = 4$	0.00518(2)	0.00518(2)
$J = 5$	0.000216(2)	0.000216(2)
$J = 6$	0.000004(1)	0.000004(1)

E. Higher spin: $S = 5/2$, 3, $7/2$, and 4

From the results of the previous four subsections, the spin-S Heisenberg model on the Husimi lattice provides one example of a gapless spin liquid, one uniform simplex-solid state, one non-uniform simplex solid, and one ordered antiferromagnet. These results imply very strong variability and an equally strong "odd-even" effect between integer and half-odd-integer spins. The complete lack of systematics to date mandates continuing the study to higher S values.

However, by considering the next four S values up to $S = 4$, we find that the ground states are all antiferromagnetically ordered with the classical 120-degree Néel configuration. The spontaneous magnetization values M are shown as a function of S in Fig. 18. Beyond $S = 2$, M clearly tends monotonically towards its classical value, S, with no evidence even for alternation effects related to the integer or half-odd-integer nature of the quantum spin. Thus "quantum effects," meaning the relevance of quantum mechanical fluctuations, really are limited to small S values ($S = 1/2$, 1, and 2), before classical physics becomes dominant. This is equally true for the half-odd-integer series, where only $S = 1/2$ is "quantum enough" to remain disordered while $S = 3/2$ is well antiferromagnetically ordered, as it is for the integer series, where only $S = 1$ and 2 have simplex-solid states more favorable than classical order.

Information about the concomitant entanglement can be obtained from the ES, which is shown in Fig. 19 for all

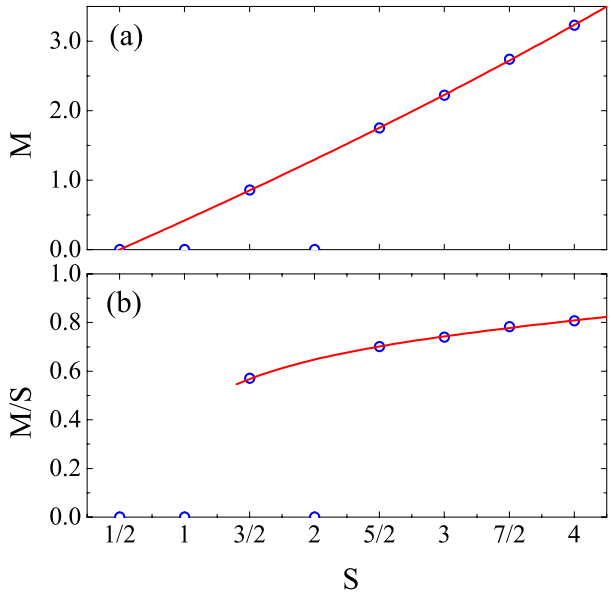

FIG. 18. (Color online) (a) Extrapolated magnetization $M(\infty)$ as a function of spin quantum number S for $S \leq 4$. (b) Ratio of extrapolated magnetization M to classical spin magnitude S. Red lines are guides to the eye.

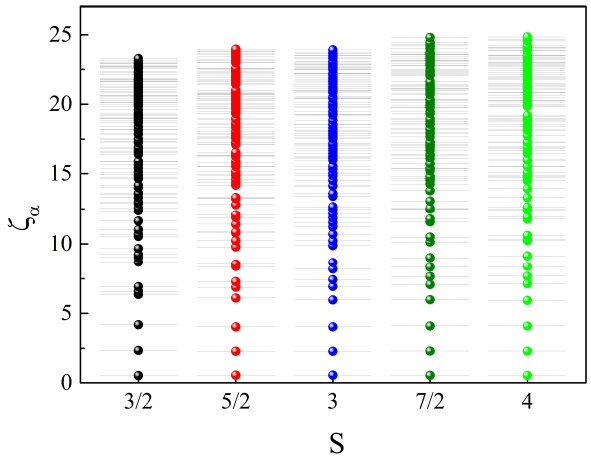

FIG. 19. (Color online) Entanglement spectra of the Heisenberg model on the Husimi lattice for $S = 3/2$, $5/2$, 3, $7/2$, and 4, calculated with bond dimension $D = 90$. All bonds are equivalent and all low-lying levels in the spectra are non-degenerate.

spins $3/2 \leq S \leq 4$. In contrast to the simplex-solid states found for $S = 1$ and 2 (Figs. 12 and 17), the structure of the ES is very simple, with all low-lying levels being non-degenerate. This indicates that the antiferromagnetically ordered state has no many-body entanglement and is effectively just a product state with short-range entanglement only. This property is a common characteristic for all magnetically ordered phases and allows us also to

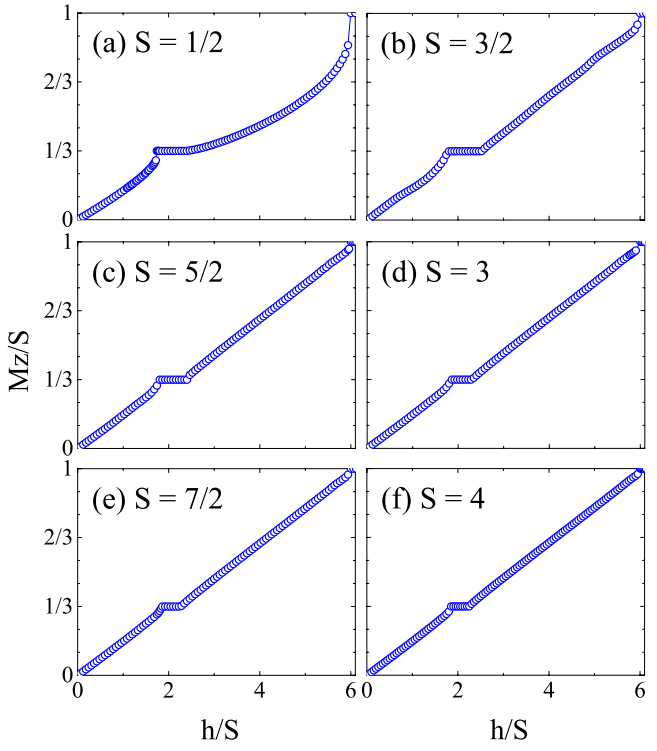

FIG. 20. (Color online) Longitudinal magnetization, M_z, normalized by its saturation value, S, as a function of external magnetic field, h, for (a) $S = 1/2$, (b) $S = 3/2$, (c) $S = 5/2$, (d) $S = 3$, (e) $S = 7/2$, and (f) $S = 4$; calculations performed with bond dimension $D = 30$. In every case, M_z rises linearly from zero with applied field, and a magnetization plateau is present at 1/3 of the saturation value.

interpret the results for the $S = 1/2$ case (Fig. 9), when we recall that this state has finite Néel order for all finite values of D.

IV. GROUND STATES WITH APPLIED MAGNETIC FIELD

A. Longitudinal Magnetization

For a deeper understanding of the nature of the Heisenberg antiferromagnet on the Husimi lattice, we have also performed a systematic investigation of the longitudinal magnetization [Eq. (11)] induced by the application of a finite magnetic field in Eq. (1), as outlined in Sec. IID3. Complete results for $S = 1/2$, $3/2$, $5/2$, 3, $7/2$, and 4 are shown in Fig. 20 and for $S = 1$ and 2 in Fig. 21. All of these calculations were performed with $D = 20$ and 30, and we find negligible changes in the results for all cases other than $S = 1/2$ and $S = 1$ and 2 at small fields. The situation for $S = 1/2$ is already understood from the results of Fig. 8; for $S = 1$ and 2, some details differ at the percent level at finite magnetizations outside the simplex-solid state (i.e. in and just beyond the insets in

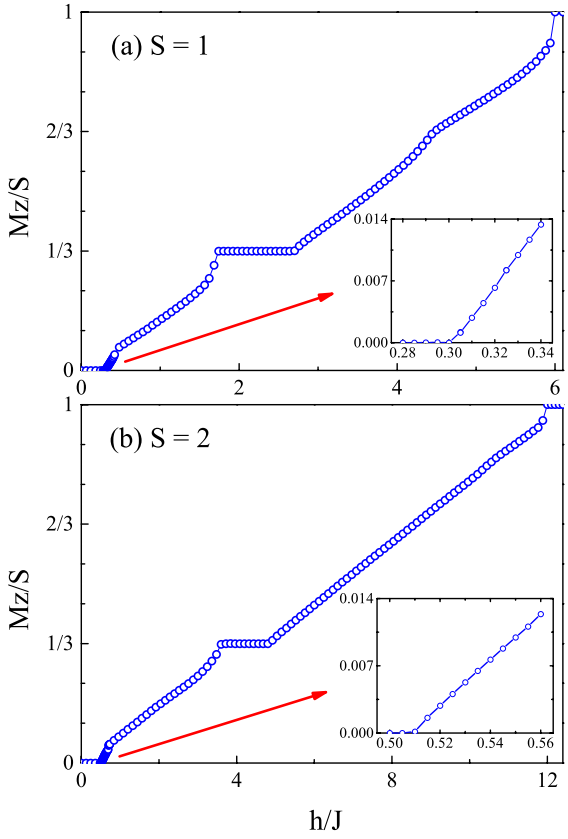

FIG. 21. (Color online) Longitudinal magnetization, M_z, normalized by its saturation value, S, as a function of external magnetic field, h, for (a) $S = 1$ and (b) $S = 2$; calculations performed with bond dimension $D = 30$. In both cases, zero induced magnetization persists up to a finite value of the applied field, indicating the presence of a spin gap $\Delta_s = h_c \simeq 0.300(5)J$ for the $S = 1$ trimerized simplex solid and $\Delta_s = h_c \simeq 0.510(5)J$ for the $S = 2$ uniform simplex solid. Both cases also show a strong plateau at 1/3 of the saturation magnetization.

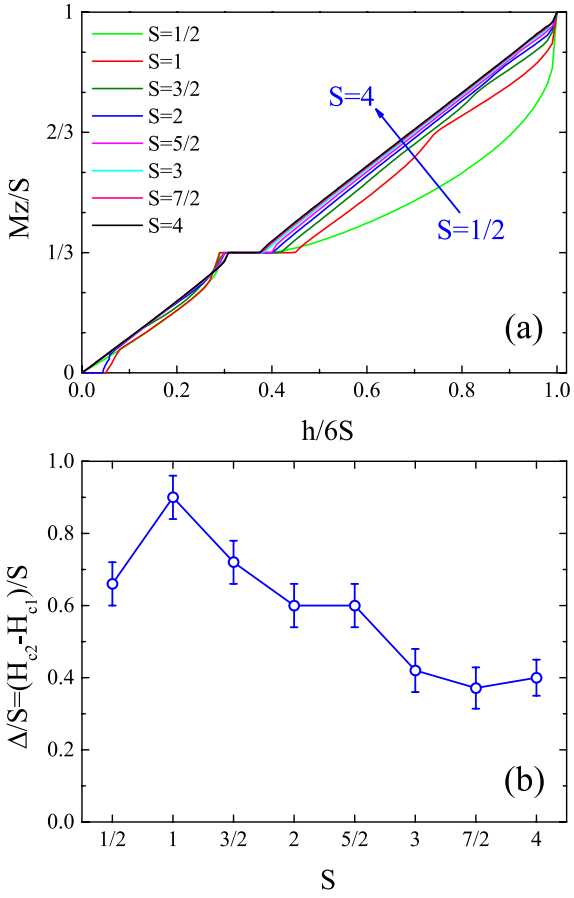

FIG. 22. (Color online) (a) Comparison of normalized longitudinal magnetization curves, $M_z(h)$, for all values of the spin quantum number, S, computed with bond dimension $D = 30$. (b) Width of the 1/3-magnetization plateau as a function of S.

Fig. 21). From these observations we conclude that all of our finite-field calculations are fully representative of the high-D limit.

At low fields, the induced magnetization, M_z, reflects directly the presence or absence of a spin gap. In its presence, no magnetization can be induced until the applied field exceeds a particular value, breaking the SU(2) symmetry. For the gapless spin-liquid state at $S = 1/2$, and for all the Néel-ordered ground states shown in Fig. 20, M_z rises linearly with h as expected. By contrast, for the simplex-solid ground states at $S = 1$ and 2 (Fig. 21), zero magnetization is found to persist until the external field exceeds a critical value, h_c, which corresponds to the spin gap [52]. For the $S = 1$ trimerized simplex solid we obtain $\Delta_s = h_c \simeq 0.300(5)$ and for the $S = 2$ uniform simplex solid $\Delta_s = h_c \simeq 0.510(5)$. We find that the transitions out of the simplex-solid states are continuous (insets, Fig. 21).

At finite values of the applied field, the most striking feature is the presence of a plateau at 1/3 of the saturation magnetizaton. This plateau is not only present for all values of the spin quantum number, S, both integer and half-odd-integer, but is broad, indicating a robust, gapped state of the magnetic system around this external field. Before investigating the nature of the 1/3-plateau state, we comment on the recovery of classical behavior with increasing S. The strongest manifestation of quantum effects appears to be the curvature in the longitudinal response above the 1/3 plateau for $S = 1/2$; for all other S values, the response is significantly more linear, as shown in Fig. 22(a). However, to recover the completely linear magnetization of the classical limit, it would be necessary for the width of the 1/3 plateau, shown in Fig. 22(b), to vanish. Clearly this situation is not imminent even at $S = 7/2$ or 4, which reflects again the robust nature of the 1/3 feature.

We comment here that that magnetization curves we have obtained for the Husimi lattice are quite similar to those obtained for the kagome lattice in a number of

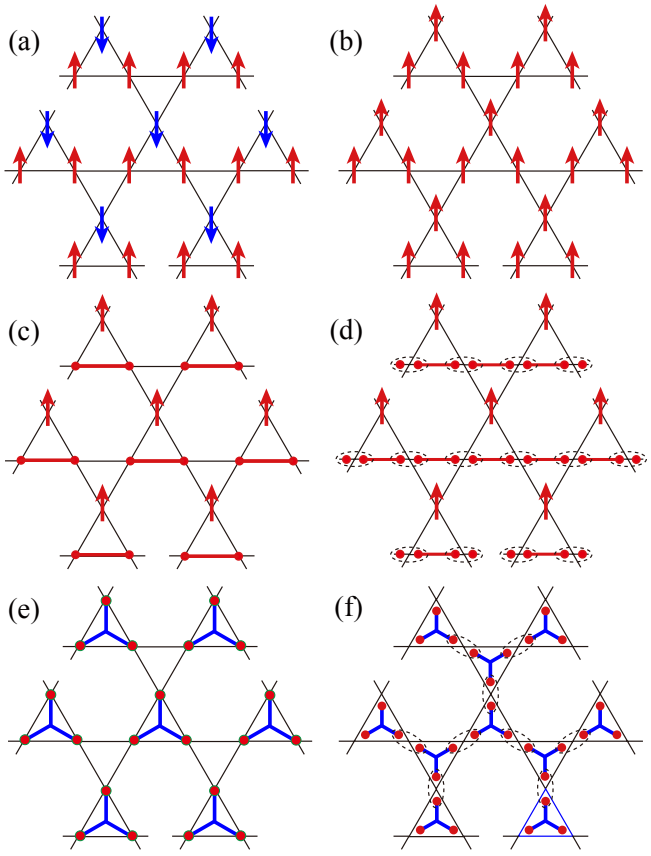

FIG. 23. (Color online) Six spin states with $m = 1/3$. (a) "Classical up-up-down" spin configuration; (b) "classical ferromagnetic" spin configuration with site moments $S/3$; (c) "type-I quantum" configuration with singlet pairs (red bonds) formed by two physical spins; (d) "type-II quantum" configuration with singlet pairs (red bonds) formed by two fractionalized virtual spins; (e) non-uniform simplex-solid state with a triplet on every up-triangle, relevant for $S = 1$; (f) uniform simplex solid state with a triplet on every simplex, relevant for $S = 2$.

recent studies by exact diagonalization [20, 53], by density matrix renormalization group [54], and by tensor-network methods based on infinite PEPS [21]. These similarities cover all the primary features of the curves, including spin gap, 1/3 plateau, and linearity, demonstrating again the extremely close parallels between the two geometries.

The primary difference between our results and those of Refs. [20, 21, 53, 54] concerns the presence on the kagome lattice of additional plateaus in multiples of 1/9 of the saturation magnetization. On the Husimi lattice, we find no $l/9$ plateaus (where l represents an integer). Magnetization plateaus generally satisfy the Oshikawa-Yamanaka-Affleck "commensurate filling" condition [55],

$$n(S - m) \quad \text{is an integer,} \tag{16}$$

where n denotes the number of sites in the unit cell and m the longitudinal magnetization. Although we do not observe the plateaus at $M_z/S = m = (1 - \frac{2}{9S})$ and $(1 - \frac{1}{9S})$ found in Refs. [21, 53, 54], a simple explanation would be that there are only three sites ($n = 3$) in the unit cell of the 3-PESS wave function used in our study. Finding these and higher plateaus would require that the tensor-network states are based at least on PESS with a 9-site unit cell, as employed in Ref. [21] within a 3-PESS formulation and in Ref. [16] using a 9-PESS. However, the fact that our current calculations should be able to find a 1/9 plateau for the $S = 3/2$ system [Eq. (16)] indicates that this is not the only factor involved. In Refs. [53] and [54], the authors explain the presence of $l/9$ plateaus on the basis of stable localized eigenstates centered on the hexagons of the kagome lattice. Thus their absence in the magnetization response of the Husimi lattice should be understood as a consequence of the absence of closed loops of triangles.

B. 1/3-Plateau State

We close our analysis of the longitudinal magnetization by investigating the nature of the 1/3-plateau state for different values of S. Our PESS results contain complete information about the quantum wave function. Many possible spin configurations could give rise to a net longitudinal magnetization $m = 1/3$, of which six are represented in Fig. 23. Some are effectively magnetically ordered [Figs. 23(a) and (b)], some are motivated by considerations of valence-bond formation [Figs. 23(c) and (d)], and some by simplex solids where the singlets may be replaced by higher-spin states [Figs. 23(e) and (f)]. These states are not necessarily orthogonal and each is only a paradigm for the dominant physics of a complex quantum superposition. The "type-I quantum" spin configuration [Fig. 23(c)], which contains a singlet pair within a single simplex (triangle), has been proposed for the $S = 1$ Heisenberg model on the kagome lattice by Cai *et al.* [25]. Both "type-I" and "type-II quantum" configurations may also be relevant to integer-spin simplex-solid states, because their ground states at zero field contain simplex singlets.

However, analyzing the PESS wave function by calculating the extent of magnetic order for various S values leads to two possibly unexpected conclusions. First, it is not necessary to consider the more exotic singlet- or simplex-based states [Figs. 23(c)–(f)] as candidates for the 1/3 plateau. As shown in Figs. 24(a), (c), (e), and (g), the dominant physics of the 1/3-plateau state is a tendency to magnetic order. This tendency does not occur in the same way in every case and it is remarkably pronounced for low spins, particularly $S = 1/2$ [Fig. 24(a)], where the approach to 1/3 magnetization is marked by a very strong and rapid rise in the ordered component; in fact the loss of the plateau state at higher fields is accompanied by a decrease in the overall degree of local spin order before a recovery with some complex behavior on the very steep approach to full saturation [Fig. 20(a)].

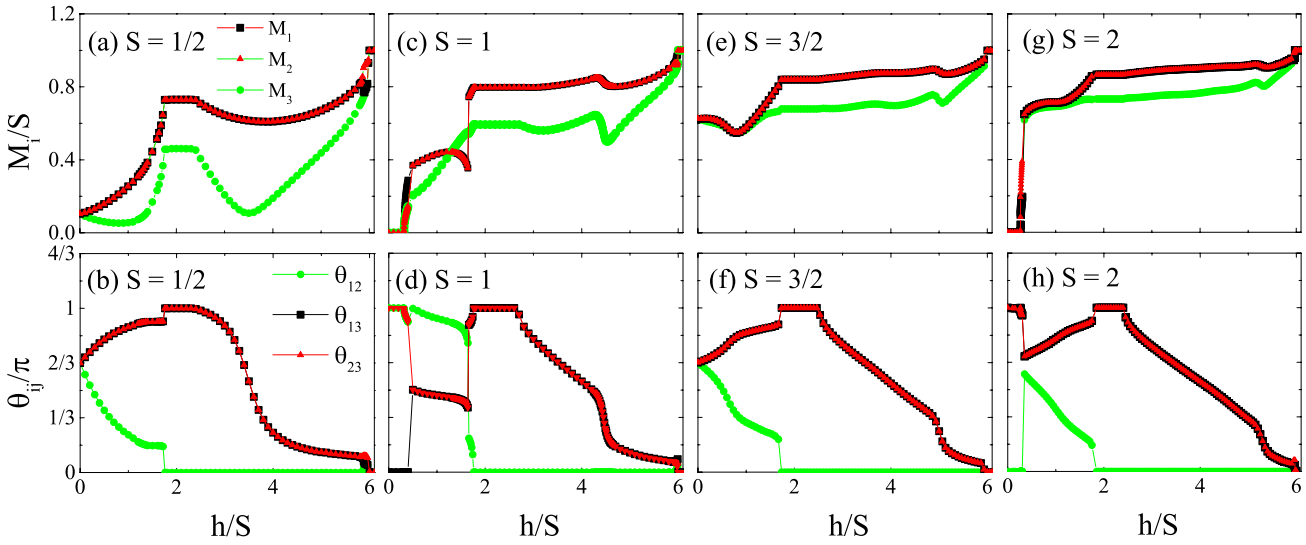

FIG. 24. (Color online) Magnetic ordering on the Husimi lattice in an applied field. Shown are the induced ordered moments, M_i, along the field (z) axis for each of the three spins on a triangle (a, c, e, g) and the relative angles, θ_{ij}, between the three pairs of spins on a triangle (b, d, f, h). The spin quantum numbers are $S = 1/2$ (a, b), $S = 1$ (c, d), $S = 3/2$ (e, f), and $S = 2$ (g, h). Calculations performed with $D = 20$.

For $S = 1$ [Fig. 24(c)], the transition from the gapped, trimerized simplex-solid state at low fields to a field-ordered state is abrupt but continuous, although the ordered moment again shows non-monotonic behavior as the 1/3 and fully aligned states are approached. For $S = 3/2$ [Fig. 24(e)], the zero-field order of all three spins actually drops with a small applied field, even as the relative spin angles change, before increasing again towards the 1/3 plateau. Beyond this, the system tends to full alignment with only small deviations around $h/S \approx 5$ (possibly marking an incipient plateau instability, which we cannot trace in the current 3-PESS formalism). For $S = 2$ [Fig. 24(g)], the ordered moments are almost homogeneous beyond the continuous transition out of the simplex-solid phase, and the degree of inhomogeneity and non-monotonic behavior is quite limited. We comment that for all spins $S \geq 5/2$ (not shown), the evolution is an increasingly homogeneous and monotonic version of our results for the Néel-ordered $S = 3/2$ state, shown in [Fig. 24(e)], as the system approaches the classical limit. Less surprising than all of this complex behavior in the inequivalent ordered moments is that the ordering configuration on the 1/3 plateau in all cases is, qualitatively, the up-up-down alignment of Fig. 23(a), as shown in Figs. 24(b), (d), (f), and (h) by the evolution of the angles between each the spin pairs on each bond. These tend to begin near 120-degree angles for all three bonds but evolve towards a situation with one parallel spin pair before the 1/3 plateau, which then remains exactly parallel all the way to saturation (Fig. 24).

Secondly, the up-up-down state departs quite significantly from the classical, rigid-spin form shown in Ref. [41]. There is an immediate and spontaneous breaking of symmetry at any finite field, or directly beyond the ordering transition for $S = 1$ and 2, where one of the three spins on each triangle becomes anti-aligned [Figs. 24(b), (d), (f), and (h)] and its ordered moment differs from the other pair. For $S = 1/2$, the average moment of this third spin actually decreases in size, while the other two grow symmetrically [Fig. 24(a)], as represented schematically in Fig. 25. The 1/3-plateau state realized for every value of S is an asymmetric one, in which the two spins aligned parallel with the field have a strong ordered component while the antiparallel spin is weakly ordered; the ordered components have no universal value, but their sum is 1/3 of the saturation value corresponding to S. On leaving the plateau state, as noted above the ordered component of the asymmetric spin shrinks in value again for $S = 1$ [Fig. 24(c)], and very dramatically for $S = 1/2$ [Fig. 24(a)], where a reduction is also visible in the symmetric spin moments, indicating that the magnetic state at higher fields becomes "more quantum"

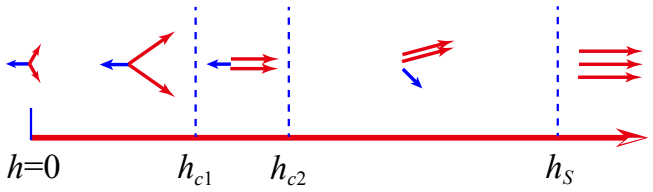

FIG. 25. (Color online) Schematic representation of the ordered spin moments and alignments on each triangle across the field-induced phase diagram for the finite-D $S = 1/2$ Heisenberg model on the Husimi lattice. The fields h_{c1} and h_{c2} mark the lower and upper boundaries of the 1/3 plateau.

again (i.e. contains more fluctuations). This behavior does not occur for any of the higher spins [$S \geq 3/2$, Figs. 24(e) and (g)], but the asymmetry in ordered moment between the lone spin and the pair persists in all cases and for all fields. The bond angles formed by each of the spin pairs [Figs. 24(b), (d), (f), and (h)] show a departure again from full up-up-down field alignment in the regime beyond the 1/3 plateau, but always with one spin pair completely parallel, as represented in Fig. 25. The process of regaining full spin alignment on the approach to saturation is not a smooth one for any value of S, with rather abrupt changes occurring at high fields, although in contrast to the ordered moments [Figs. 24(c), (e), and (g)], it is monotonic in the bond angles [Figs. 24(d), (f), and (h)].

We observe that the field-induced magnetization curves show a complex interplay of a number of quantum fluctuation phenomena. Clearly the spin configurations in the 1/3-plateau state have significant components of the "up-up-down" structure for every value of S, even in the most quantum cases and those most susceptible to simplex-solid formation. However, this is not precisely the classical configuration of Ref. [41] but an asymmetric version of it, with one suppressed spin and two extended ones (Fig. 25). The degree of up-up-down order is therefore not a perfectly defined quantity, although a relative degree could certainly be obtained by comparing only the order of the strong components, or of the weak ones. We comment that the unequal ordered moments in the graphic of Fig. 25 are strongly exaggerated for $S = 3/2$ and $S \geq 5/2$, and would be modified by the simplex-solid (zero-magnetization) states appearing at low fields for $S = 1$ and $S = 2$. For $S = 1/2$, this picture is strictly valid only for our results at finite values of D, because the ordered moment at $h = 0$ vanishes in the limit $D \to \infty$, but is representative at all finite fields. We expect this schematic to be accurate in all its details for the phase diagram of the $S = 1/2$ Heisenberg model on the triangular lattice, which does possess 120^0-degree Néel order at $h = 0$.

We conclude that the application of a magnetic field is particularly effective in quenching quantum fluctuation phenomena, driving the system rapidly to states dominated by magnetic order. However, quantum fluctuation effects remain very apparent in the clear preference for collinear spin alignment, manifested in the existence of a robust and well ordered 1/3 plateau for all S values. This effect, which is remarkably strong for $S = 1/2$, is presumably due to the fully antiferromagnetic quantum fluctuations allowed between collinear spins. Below collinear configurations in priority, coplanar ordered spin states remain preferred over non-coplanar ones.

V. SUMMARY

We have investigated the antiferromagnetic Heisenberg model on the triangular Husimi lattice for values of the quantum spin S up to $S = 4$. We made use of tensor-network techniques based on Projected Entangled Simplex States (PESS) to work directly in the thermodynamic limit for highly frustrated systems. The bisimplex Husimi geometry makes a simple-update approach to evaluating the quantum wave function almost exact, enabling us to obtain systematic and highly accurate results to very large values ($D = 260$) of the bond dimension, and thus to be certain of the trends contained in our data.

We have demonstrated that the ground state of the model varies widely with S, presenting for $S = 1/2$, 1, 3/2, and 2 excellent examples of four quite different quantum states. For $S = 1/2$ the ground state is a gapless (algebraic) spin liquid; for $S = 1$, it is a trimerized (non-uniform) simplex-solid state with a spin gap; for $S = 3/2$ it is an antiferromagnet with classical (120-degree) triangular Néel order; for $S = 2$, it is a (uniform) simplex-solid state and therefore is again gapped. However, these dramatic quantum effects are quenched very rapidly by increasing S, and all higher-spin cases are ordered antiferromagnets, whose ordered moments increase monotonically with S.

One property of a system readily calculated from its tensor-network wave function is the entanglement spectrum. For the ground states with Néel order, the entanglement spectrum is simple, with all low-lying levels being non-degenerate, and this result applies also to the gapless spin-liquid state obtained for $S = 1/2$, which has finite order at all finite values of D. By contrast, the entanglement spectra of the simplex-solid states found for $S = 1$ and 2 are clearly different, being characterized by specific degeneracies in their low-energy levels. Our results suggest that the entanglement spectrum offers a valuable means of distinguishing between different types of complex quantum state.

A further quantity readily computed in the PESS framework is the magnetization response to an external field. We find predictable results at low fields, with a linear response for the ordered phases and the gapless spin liquid but a clear spin gap for the simplex-solid states. Surprisingly, however, no matter how different the low-field quantum states, we find a magnetization plateau at 1/3 of the saturation value for all values of S. This ubiquitous feature even has the same origin in every case, namely a significant component of the semiclassical, but asymmetric, "up-up-down" configuration on every triangle. We suggest that the universality of this phenomenon can be traced to the strong tendency of antiferromagnetic fluctuations to favor collinear spin alignments.

When considering our results for $S = 1/2$, 1, and 2, it is tempting to seek a parallel with the Haldane conjecture, that perhaps half-odd-integer-spin Husimi lattices may be gapless spin liquids whereas integer-spin ones are simplex solids. However, the rapid emergence of antiferromagnetically ordered states at (all) higher S values in both series demonstrates that the predominant physics of the Husimi lattice is two-dimensional. That this result

applies even for a geometry as "quasi-one-dimensional" as the Bethe lattice of triangles allows us to conclude that the dominant effects on the Husimi lattice are intrinsic to the triangle, and to its local coordination by only three other triangles, rather than to any features of the open, tree-like structure.

Persisting with the view of the Husimi lattice as a Bethe lattice of triangles offers a possible interpretation of our result that the $S = 1/2$ system is a gapless spin liquid. The $S = 1/2$ triangle has two degenerate doublets and therefore the model may be analogous to a two-color $S = 1/2$ Bethe lattice. The conventional $S = 1/2$ Bethe lattice has been considered in Ref. [56], where it was found that both the Ising and XY versions of the model have long-ranged magnetic order, but with orthogonal alignments. The Heisenberg point therefore appears as the transition between different magnetic states, which is definitely consistent with our finding of a gapless spin liquid. This very delicate balance is not reproduced for any other values of S.

Returning to the issue of how weak quantum mechanical fluctuation effects appear to be on the Husimi lattice, as noted in Secs. IIIE and IV we have found that they are restricted to three very small values of S and to low applied fields. On one hand it is perhaps dispiriting in the search for exotic quantum states that their phase space is so small even for the Husimi lattice, which due to its very low coordination and low inter-triangle connectivity should be a very "quantum" geometry. On the other hand, however, the low connectivity in this case results in relatively low frustration, restricting it to intra-triangle effects, and this observation reinforces the fact that the recipe for non-trivial quantum phenomena requires as essential ingredients both low spin and high frustration.

Finally, we revisit the question of whether our results for the Husimi lattice shed any important new light on the vexed question of the quantum ground states of the kagome lattice. All of the properties we have found for the spin-S Husimi antiferromagnets, including energies, order parameters, and induced magnetizations, are remarkably similar (both qualitatively and quantitatively) to those of the kagome lattice where these are known. Clearly the local structure of corner-sharing triangles determines the vast majority of the physics, and this is sufficient to cement the parallel in all but the most delicate cases. Setting aside the higher-spin examples, where the systems are almost identical [21], in this discussion we focus only on $S = 1$ and $S = 1/2$.

For the $S = 1$ Husimi lattice, our result that the ground state is a trimerized simplex solid follows mere months after the demonstration, by two different techniques [26, 27], that the same type of state has the lowest energy yet obtained for the $S = 1$ kagome lattice. We suggest that the entanglement spectrum could be used for a definitive identification of this state. Our results add important new evidence that such spontaneous breaking of translational symmetry, in the formation of alternating simplex types, may indeed be the generic physics of the $S = 1$ system.

For the $S = 1/2$ case, our result that the ground state of the Husimi lattice is a gapless spin liquid requires a more careful interpretation. The existence of closed loops of triangles in the kagome geometry, which are absent in the Husimi case, means that geometrical frustration on the kagome lattice is stronger. Quantum fluctuation effects should therefore suppress more strongly the magnetic order we find at finite values of the bond dimension. However, whether this suppression retains a stronger algebraic form, characteristic of a gapless spin liquid, or turns over to the exponential form characteristic of a gapped spin liquid, remains the crucial open question unanswered by the present study.

ACKNOWLEDGMENTS

We thank W. Li for helpful discussions and J. Richter for valuable comments. This work was supported by the National Natural Science Foundation of China (Grant Nos. 10934008, 10874215, and 11174365) and by the National Basic Research Program of China (Grant Nos. 2012CB921704 and 2011CB309703).

[1] F. D. M. Haldane, Phys. Lett. A **93**, 464 (1983).
[2] F. D. M. Haldane, Phys. Rev. Lett. **50**, 1153 (1983).
[3] E. H. Lieb, T. D. Schultz, and D. C. Mattis, Ann. Phys. (NY) **16**, 407 (1961).
[4] I. Affleck and E. H. Lieb, Lett. Math. Phys., **12**, 57 (1986).
[5] I. Affleck, T. Kennedy, E. H. Lieb, and H. Tasaki, Phys. Rev. Lett. **59**, 799 (1987).
[6] I. Affleck, T. Kennedy, E. H. Lieb, and H. Tasaki, Commun. Math. Phys. **115**, 477 (1988).
[7] M. den Nijs and K. Rommelse, Phys. Rev. B **40**, 4709 (1989).
[8] E. Berg, E. G. Dalla Torre, T. Giamarchi, and E. Altman, Phys. Rev. B **77**, 245119 (2008).
[9] Z.-C. Gu and X.-G. Wen, Phys. Rev. B **80**, 155131 (2009).
[10] X. Chen, Z.-C. Gu, and X.-G. Wen, Phys. Rev. B **83**, 035107 (2011).
[11] X. Chen, Z.-C. Gu, and X.-G. Wen, Phys. Rev. B **84**, 235128 (2011)
[12] N. Schuch, D. Perez-Garcia, and I. Cirac, Phys. Rev. B **84**, 165139 (2011).
[13] X. Chen, Z.-C. Gu, Z.-X. Liu, and X.-G. Wen, Phys. Rev. B **87**, 155114 (2013).
[14] M. B. Hastings, Phys. Rev. B, **69**, 104431 (2004).
[15] D. P. Arovas, Phys. Rev. B **77**, 104404 (2008).
[16] Z.-Y. Xie, J. Chen, J.-F. Yu, X. Kong, B. Normand, and T. Xiang, Phys. Rev. X **4**, 011025 (2014).

[17] C. Zeng and V. Elser, Phys. Rev. B **42**, 8436 (1990); J. B. Marston and C. Zeng, J. Appl. Phys. **69**, 5962 (1991); P. Nikolic and T. Senthil, Phys. Rev. B **68**, 214415 (2003); R. R. P. Singh and D. A. Huse, Phys. Rev. B **76**, 180407 (2007); R. R. P. Singh and D. A. Huse, Phys. Rev. B **77**, 144415 (2008); G. Evenbly and G. Vidal, Phys. Rev. Lett. **104**, 187203 (2010); Y. Iqbal, F. Becca, and D. Poilblanc, Phys. Rev. B **83**, 100404 (2011).

[18] S. Sachdev, Phys. Rev. B **45**, 12377 (1992); H. C. Jiang, Z. Y. Weng, and D. N. Sheng, Phys. Rev. Lett. **101**, 117203 (2008); S. Yan, D. A. Huse, and S. R. White, Science **332**, 1173 (2011); S. Depenbrock, I. P. McCulloch, and U. Schollwock, Phys. Rev. Lett. **109**, 067201 (2012); H. C. Jiang, Z. H. Wang, and L. Balents, Nat. Phys. **8**, 902 (2012).

[19] Y. Ran, M. Hermele, P. A. Lee, and X. G. Wen, Phys. Rev. Lett. **98**, 117205 (2007); Y. Iqbal, F. Becca, S. Sorella, and D. Poilblanc, Phys. Rev. B **87**, 060405 (2013).

[20] H. Nakano and T. Sakai, J. Phys. Soc. Jpn. **84**, 063705 (2015).

[21] T. Picot, M. Ziegler, R. Orus, and D. Poilblanc, Phys. Rev. B **93**, 060407(R) (2016).

[22] K. Hida, J. Phys. Soc. Jpn. **69**, 4003 (2000).

[23] H. Yao, L. Fu, and X.-L. Qi, unpublished (arXiv:1012.4470).

[24] W. Li, S. Yang, M. Cheng, Z.-X. Liu, and H.-H. Tu, Phys. Rev. B **89**, 174411 (2014).

[25] Z. Cai, S. Chen, and Y. P. Wang, J. Phys.: Condens. Matter, **21**, 456009 (2009).

[26] T. Liu, W. Li, A. Weichselbaum, J. von Delft, and G. Su, Phys. Rev. B **91**, 060403(R) (2015).

[27] H. J. Changlani and A. M. Lauchli, Phys. Rev. B **91**, 100407(R) (2015).

[28] O. Gotze, D. J. J. Farnell, R. F. Bishop, P. H. Y. Li, and J. Richter, Phys. Rev. B **84**, 224428 (2011).

[29] K. Husimi, J. Chem. Phys. **18**, 682 (1950).

[30] C. L. Henley, Can. J. of Phys. **79**, 1307 (2001).

[31] H. C. Jiang, Z. Y. Weng, and T. Xiang, Phys. Rev. Lett. **101**, 090603 (2008).

[32] W. Li, J. von Delft, and T. Xiang, Phys. Rev. B **86**, 195137 (2012).

[33] V. Elser and C. Zeng, Phys. Rev. B **48**, 13647 (1993).

[34] Z. Hao and O. Tchernyshyov, Phys. Rev. Lett. **103**, 187203 (2009).

[35] R. J. Riddell, and G. E. Uhlenbeck, J. Chem. Phys. **21**, 2056 (1953).

[36] F. Harary and G. E. Uhlenbeck, Proc. Natl. Acad. Sci. U.S. **39**, 315 (1953).

[37] A. Cayley, Amer. J. Math. (2): 174 (1878).

[38] J. De Miranda-Neto and F. Moraes, J. Phys. I France **3**, 29 (1993).

[39] M. Ostilli, Physica A **391**, 3417 (2012).

[40] F. Verstraete and J. I. Cirac, unpublished (arXiv:cond-mat/0407066).

[41] M. Takigawa and F. Mila, in *Introduction to Frustrated Magnetism*, eds. C. Lacroix, P. Mendels, and F. Mila (Springer, Heidelberg, 2011).

[42] Z. Y. Xie, H. C. Jiang, Q. N. Chen, Z. Y. Weng, and T. Xiang, Phys. Rev. Lett. **103**, 160601 (2009).

[43] H. H. Zhao, Z. Y. Xie, Q. N. Chen, Z. C. Wei, J. W. Cai, and T. Xiang, Phys. Rev. B **81**, 174411 (2010).

[44] G. Vidal, Phys. Rev. Lett. **91**, 147902 (2003); G. Vidal, Phys. Rev. Lett. **93**, 040502 (2004).

[45] S. Depenbrock and F. Pollmann, Phys. Rev. B **88**, 035138 (2013).

[46] Z. Y. Xie, J. Chen, M. P. Qin, J. W. Zhu, L. P. Yang, and T. Xiang, Phys. Rev. B **86**, 045139 (2012).

[47] L. de Lathauwer, B. de Moor, and J. Vandewalle, SIAM J. Matrix Anal. Appl. **21**, 1253 (2000).

[48] H. Li and F. D. M. Haldane, Phys. Rev. Lett. **101**, 010504 (2008).

[49] X.-Y. Deng, L.-J. Kong, and L. Qiang, Eur. Phys. J. B **87**, 247 (2014).

[50] T. Liu, S.-J. Ran, W. Li, X. Yan, Y. Zhao, and G. Su, Phys. Rev. B **89**, 054426 (2014).

[51] N. D. Mermin and H. Wagner, Phys. Rev. Lett. **17**, 1133 (1966).

[52] A. Garcia-Saez, V. Murg, and T.-C. Wei, Phys. Rev. B **88**, 245118 (2013).

[53] S. Capponi, O. Derzhko, A. Honecker, A. M. Läuchli, and J. Richter, Phys. Rev. B **88**, 144416 (2013).

[54] S. Nishimoto, N. Shibata and C. Hotta, Nat. Commun. **4**, 2287 (2013).

[55] M. Oshikawa, M. Yamanaka, and I. Affleck, Phys. Rev. Lett. **78**, 1984 (1997); M. Oshikawa, Phys. Rev. Lett. **90**, 236401 (2003).

[56] H. Otsuka, Phys. Rev. B **53**, 14004 (1996).